A Sulfur Isotopic Study of Neoproterozoic Evaporites in the Shaler Supergroup, Victoria Island, Northwest Territories, Canada

Brendan P. Williams

Advisors: Dr. Alan J. Kaufman and David T. Johnston

GEOL 394 Final Paper

Abstract

Sulfur isotopes are valuable indicators of microbial metabolisms, and are sensitive to the oxidation state of the Earth's surface. The Shaler Supergroup, which is located on Victoria Island in the Northwest Territories of Canada, is comprised of predominantly carbonates, shales, and evaporites, and was deposited on a broad tectonically stable low gradient, shallow marine platform within the intracratonic Amundsen Basin. Considering sulfate's long residence time in the oceans, and subsequent isotopic homogenization, sulfate minerals, such as evaporites, are an ideal reservoir to examine the oxidative sulfur cycle. In this study, sulfur isotope measurements (^{32}S, ^{33}S, and ^{34}S) of the Shaler Supergroup bedded evaporites suggest active communities of sulfur disproportionating bacteria, indicating that the oxidative sulfur cycle was operating in the early Neoproterozoic Era. The data have led to additional questions about the potential effect of restricted basin dynamics. In addition to the sulfur isotope measurements, this study draws from previous work on C, O, and Sr isotopes to aid in our understanding of the Shaler Supergroup depositional environment. Previous work suggests that the Shaler Supergroup may record evidence of preglacial trends corresponding to the earliest Neoproterozoic snowball Earth event.

Table of Contents **Page Number**

List of Figures

Introduction

The Neoproterozoic Era is notable in the geologic record as a time of great instability. Major Neoproterozoic events include: 1) the amalgamation and breakup of large supercontinents, (Hoffman, 1991; Dalziel, 1997; Karlstrom *et al.,* 2000), 2) innovations and mass extinctions of biological communities, 3) multiple and widespread glaciations (Kirschvink, 1992; Hoffman *et al.,* 1998) and 4) significant variations in the sulfur, carbon, oxygen, and strontium isotopic compositions of the oceans (Asmerom *et al.,* 1991; Kaufman and Knoll, 1995; Canfield, 2001; Hurtgen *et al.,* 2002). These isotope systems aid in the interpretation of extreme environmental change in the Neoproterozoic. More specifically, sulfur isotopes track microbial activity and are sensitive to the oxidation state of the surface both in the global ocean and local depositional environments.

In the marine setting, the dominant sulfur reservoirs are seawater sulfate (SO_4^{2-}), calcium sulfate in evaporites ($CaSO_4$), and pyrite (FeS_2). Sulfate is the second most abundant anion in modern seawater, and is a significant oxidant of organic matter via microbial sulfate reductions. This biological process leads to the formation of ^{34}S depleted hydrogen sulfide (H_2S), which is sequestered in sediments as pyrite. Conversely, the evaporite precipitation of overlying seawater records the isotopic compositions (Strauss, 1997). In the absence of evaporites, the way to provide additional chemostratigraphic data could be measured through the extraction and analysis of trace sulfate found within the crystal lattice of carbonates (Lyons, 2004; Hurtgen *et al.,* 2005). Through the examination of this reservoir, it may be possible to estimate magnitudes of sulfur cycle change and thus infer environmental change. In order to evaluate global processes during the Neoproterozoic, we examine proxies for seawater sulfate, since sulfate is thought to be globally representative.

Sulfur Systematics

Sulfur has four naturally occurring stable isotopes (although we only report three); ^{32}S is the most abundant at 95.02%, ^{33}S at 0.760%, and ^{34}S at 4.22% (Canfield, 2001; Strauss, 1997). Based on thermodynamic principles, the definition of isotopic fractionation is the partial separation of the light from heavy isotopes during chemical or biological reactions. The relative abundances of these isotopes can change as they are biologically and abiologically cycled between reservoirs. The fractionations associated with these changes are variable depending upon the process responsible for isotopic exchange (kinetic or equilibrium isotope effects), and reported using standard delta notation where,

$$\delta^{34}S = \left(\frac{\left(\frac{^{34}S}{^{32}S} \right)_{sample}}{\left(\frac{^{34}S}{^{32}S} \right)_{reference}} - 1 \right) \times 1000 .$$

Fractionations in the less abundant isotopes (^{33}S) are noted as deviations from a reference mass fractionation line, and are expressed as

$$\Delta^{33}S = \delta^{33}S - \left[\left(1+\frac{\delta^{34}S}{1000}\right)^{\lambda_{RFL}} - 1\right] * 1000,$$

where $\lambda_{RFL} = 0.515$ for ^{33}S (Hulston and Thode 1965). These equations are based on thermodynamic relationships and mass dependent fractionation laws (Farquhar *et al.,* 2003; Schauble, 2004). Equilibrium mass dependent fractionation between $\delta^{33}S$ and $\delta^{34}S$ predicts a 0.515 relationship (Hulston and Thode 1965). Biological fractionations are inconsistent with the narrow range suggested from equilibrium studies, with slopes ranging from 0.510 to 0.518 (Johnston *et al.,* 2005b).

Sulfur Cycle

An understanding of the sulfur cycle and associated fractionations is needed in order to understand how sulfur isotope fractionations are produced and preserved within various reservoirs (Figure 1). Sulfate input to the oceans is controlled by the oxidative weathering of continental materials, including pyrite, organic sulfur, and bedded evaporites and transported through riverine processes (Strauss, 1997; Canfield and Raiswell, 1999; Hurtgen *et al.,* 2002; Hurtgen *et al.,* 2004). This sulfate could be bound in the structure of carbonates, directly precipitated as sulfate minerals (like evaporites), or consumed by sulfate reducing bacteria and become hydrogen sulfide. Once the sulfate is reduced to hydrogen sulfide, it could form pyrite or be reoxidized to a sulfur intermediate (elemental sulfur, thiosulfate, or sulfite). Sulfur disproportionating bacteria can biologically divide the sulfur intermediates into sulfate or hydrogen sulfide.

Further, some bacteria use sulfate as a terminal electron acceptor and consume simple organic molecules to produce energy and hydrogen sulfide. The free sulfide may combine with ferrous iron to form sedimentary pyrite, which constitutes a major sulfur sink. Sulfide can also be utilized by photosynthetic and nonphotosynthetic bacteria that oxidize sulfide to sulfate with molecular oxygen or nitrate (Habicht *et al.,* 1998). Observe that Figure 1 is a box model that illustrates possible processes that transfer sulfur bearing species between surface reservoirs. The fractionation associated with the precipitation of evaporites is small (Thode and Monster 1965), whereas the fractionations associated with bacterial sulfate reduction and sulfur disproportionation can be relatively large (see below).

Microbial Metabolisms

Sulfate reducing bacteria are obligate anaerobes that oxidize simple organic compounds (such as lactate and acetate) with sulfate, yielding energy (ATP) and hydrogen sulfide (Detmers *et al.,* 2001). Sulfate reducing bacteria have been known to exist since the mid Archean (Ohmoto *et al.,* 1993; Shen *et al.,* 2001). Sulfate reducing bacteria preferentially incorporate the lighter ^{32}S isotope over the heavy ^{34}S isotope, which results in hydrogen sulfide that is depleted in ^{34}S (Strauss, 1997; Canfield, 2001; Hurtgen *et al.,* 2002). The same principles apply to ^{33}S fractionations (Johnston *et al.,*

2005a). The range of $\delta^{34}S$ fractionations observed by bacterial sulfate reduction is up to 46‰ (Harrison and Thode, 1958; Kaplan and Rittenburg, 1964; Kemp and Thode, 1968; Chambers *et al.,* 1976; Canfield, 2001).

The wide range of fractionation is a function of sulfate availability, substrate availability, and temperature. Small magnitude fractionations, such as seen in the Archean, are the result of low sulfate concentrations (Habicht *et al.,* 2002). Low sulfate concentrations reduce the availability of sulfate, thereby limiting enzymatic fractionation. In contrast, if sulfate is abundant, the enzymatic preference for the light isotope can be fully expressed by these bacteria. In the modern marine system, these bacteria live within the anoxic sediment, but Holser (1977) suggests that this reduction process could take place in an anoxic (sulfidic) water column. However, as observed in the modern oceans, 90% of the sulfide produced by sulfate reduction within marine sediments is reoxidized by chemical or biological processes (Neretin *et al.,* 2001).

Microbial sulfur disproportionation, the primary metabolism in the modern oxidative sulfur cycle, requires intermediate sulfur species (elemental sulfur (S^0), thiosulfate ($S_2O_3^{2-}$), or sulfite (SO_3^{2-})) and produces both hydrogen sulfide and sulfate. The formation of intermediate sulfur species occurs through the oxidation of hydrogen sulfide originally produced from bacterial sulfate reduction (Canfield, 2001). Since these microbes are using hydrogen sulfide that is already fractionated from the starting sulfate, the residual sulfide from disproportionation reactions may be even more depleted in the heavy isotope, in $\delta^{34}S$ up to 71‰ (Thamdrup *et al.,* 1993; Canfield and Teske, 1996 Habicht *et al.,* 1998; Habicht and Canfield, 2002).

Evidence ($\delta^{34}S$) for widespread sulfur disproportionation first became apparent in the Neoproterozoic (around 800 Ma.), and was noted by an increased range of $\delta^{34}S$ values in sedimentary pyrite beyond that possible by sulfate reducing bacteria alone (Canfield and Teske, 1996). Figure 2 displays the large variations in the sulfur isotopic record throughout time, where the diamonds represent the isotopic composition of sedimentary sulfides (Canfield and Teske, 1996). The upper band represents the modeled isotopic composition of seawater sulfate (given the general absence of sulfate deposits in the Precambrian) and the lower line represents the mean of the seawater sulfate reservoir displaced by 55‰ (Canfield and Teske, 1996). The greater range in $\delta^{34}S$ values is interpreted as resulting from the onset of sulfur disproportionation and the modern oxidative sulfur cycle due to the rise of atmospheric oxygen and oxidation of the deep ocean (Canfield, 1998). However, a recent study of the minor sulfur isotopes suggests that disproportionation reactions became apparent in the geologic record at around 1300 Ma. (Johnston *et al.,* 2005a), and further suggest progressive oxygenation preceding the Neoproterozoic.

Hypothesis

In this study we report the sulfur isotopic composition of bedded evaporites from the >723 Ma Shaler Supergroup, whose deposition is temporally consistent with the marked increase in $\delta^{34}S$ values of sedimentary sulfides. These sulfates may have been

deposited as the direct result of surface oxidation, which would have also allowed for the onset of pervasive sulfur disproportionation. We hypothesize that the minor sulfur isotopes in these oxidized reservoirs will allow for testing of the presence and relative importance of sulfur disproportionating reactions in the Neoproterozoic Era.

Geologic Setting

The Shaler Supergroup, located on Victoria Island in the Northwest Territories of Canada, is made up of predominantly sedimentary facies (carbonates, shales, and evaporites) (Figure 3ab). The various formations and groups that make up the Shaler Supergroup are the Rae Group, Reynolds Point Group, Minto Inlet Formation, Wynniatt Formation, and Kilian Formation (Rainbird *et al.,* 1994) (Figure 4). These units, which totaled are ~5000 m thick, were deposited on a broad, tectonically stable, low gradient, shallow marine platform within the intracratonic Amundsen Basin (Young, 1981; Rainbird *et al.,* 1996). Because of the great thickness of the unit, the Shaler Supergroup is believed to have been deposited on a thermally subsiding continental margin adjacent to the open ocean, although restriction during evaporite deposition is likely (Young, 1981). Thick, continuously bedded evaporites deposited in the Minto Inlet and Kilian formations are the primary focus of this study. Radiometric age constraints on the Neoproterozoic Shaler Supergroup are provided by the Franklin diabase dikes and sills, which cross cut these rocks. The dikes and sills have been dated to 723 +4/-2 Ma (Rainbird *et al.,* 1996). The lower age limit of this group is 1077 ± 4 Ma, which was established by U-Pb dating of detrital zircons in the Rae Group within the Shaler Supergroup (Rainbird *et al.,* 1996).

Previous studies of carbon, oxygen, and strontium isotopes aid our understanding of depositional environments of the Shaler Supergroup (Figure 4). Carbon isotopic shifts are generally interpreted to be the result of changes in the proportional burial of organic carbon to carbonate carbon in sediments (Kaufman and Knoll, 1995). Marine carbonates become more enriched in ^{13}C (and hence have a more positive $\delta^{13}C$ value) as the amount of organic carbon buried increases. Alternatively, negative $\delta^{13}C$ values in marine carbonates would represent a decrease in the amount of organic carbon that is buried (Hoefs, 2004). Oxygen isotopes are used to track alteration, among other things diagenetic fluids. Oxygen isotope data that is consistent, without large variations, indicate unaltered material. While inconsistent oxygen isotope data indicate alteration. In carbonates, oxygen isotope signatures ($\delta^{18}O$ values) can be used to distinguish between open marine and restricted environments if the rocks have not been affected by diagenetic fluids that are of a different composition than that of seawater. There are two primary sources of strontium in seawater that affects its isotopic composition: 1) the weathering and transport of ^{87}Sr enriched continental material (from the long term decay of ^{87}Rb in granitic rocks), and 2) input of ^{87}Sr depleted mantle fluids by means of hydrothermal circulation through rift zones (Asmerom *et al.,* 1991). Low observed marine $^{87}Sr/^{86}Sr$ values suggest high hydrothermal activity perhaps related to rifting events, whereas relatively high $^{87}Sr/^{86}Sr$ would suggest high riverine inputs due to collisional events. Using this framework, Sr isotopes can be used to track active weathering rates (or a stoppage of weathering) and sources of material.

Figure 4 shows the chemostratigraphy of carbon, oxygen, and strontium isotopes plotted against depth in the Shaler Supergroup. The $\delta^{13}C$ values from the Rae Group to the Wynniatt Formation show a positive trend from about +2 to +6‰ (Kaufman and Knoll, 1995). This can be interpreted as an increasing proportion of organic carbon burial through this interval. There is a dramatic negative shift in the $\delta^{13}C$ values from the Wynniatt Formation to the Kilian Formation, with values falling from +3‰ to as low as -6‰. Negative carbon isotope shifts of this magnitude are observed in immediately pre-glacial carbonates suggesting that the Kilian Formation may precede Neoproterozoic glacial events (Kaufman and Knoll, 1995; Kaufman *et al.,* 1997; Halverson *et al.,* 2004; Hoffman *et al.,* 1998; James *et al.,* 2001).

The oxygen isotopes in the carbonates of the Shaler Supergroup in Figure 4 are depleted in $\delta^{18}O$, ranging between -2 and -10‰. There are no systematic trends in this data, although it is notable that the carbonates of the Minto Inlet Formation are relatively more enriched in ^{18}O, which may be interpreted as due to enhanced evaporation or higher temperatures of the basin waters. In general, the oxygen isotopes do not indicate any significant secondary overprinting.

The low $^{87}Sr/^{86}Sr$ values for the Shaler Supergroup marine carbonates (ca. 0.7055) suggest high hydrothermal inputs of Sr to seawater (Asmerom *et al.,* 1991). These high hydrothermal inputs would have delivered reduced fluids and ferrous iron to seawater promoting widespread bottom water anoxia. These data also could suggest a reduction or stoppage in the continental weathering rates and subsequent transport into the oceans.

Methods

The primary chemical technique involves the reduction of evaporite minerals to Ag_2S (silver sulfide) and subsequent measurement by 1) elemental analysis isotope ratio mass spectrometry (EA-IRMS) or 2) by conversion to SF_6 (sulfur hexafluoride) for dual inlet isotope ratio mass spectrometry (DI-IRMS).

Reduction of evaporite minerals to Ag_2S was modified from Thode *et al.,* (1961). Evaporites were provided by A. J. Kaufman and A. Knoll (Harvard). Samples were crushed into a fine powder in preparation for chemical preparation ($CaSO_4*2H_2O$ to Ag_2S). Ten mg of rock powder was weighed out in a 50 ml Kimax boiling flask, and is then attached to a distillation line, which was used to reduce $CaSO_4*2H_2O$ to Ag_2S. The reaction takes place in a nitrogen atmosphere, at a flow rate of about 2 bubbles per second. The reduction chemistry is catalyzed by heat and run ~100°C. A strongly reducing acid mixture (Thode solution; Thode *et al.,* 1961) reduced SO_4 to H_2S, which was bubbled through a CdAc * $2H_2O$ (cadmium acetate) or ZnAc * $2H_2O$ (zinc acetate) trap where it reacted to form CdS (cadmium sulfide) or ZnS (zinc sulfide). $AgNO_3$ is then added to the trap, to precipitate Ag_2S. In order to isolate the Ag_2S the solution and precipitate was filtered. Once the Ag_2S was isolated, it was dried prior to analysis for $\delta^{33}S$ and $\delta^{34}S$.

Analysis of 100 μg Ag_2S (and approximately one mg of V_2O_5 (vanadium pentoxide, which was added for increased oxidation efficiency) on the Micromass Isoprime continuous flow gas source mass spectrometer with an inline Elemental Analyzer was performed for preliminary $\delta^{34}S$ results. The sample was placed into the auto sampler and injected into the combustion column with He, where it flash combusted at 1030°C, producing SO_2 (sulfur dioxide) gas. The sample then flowed through a $Mg(ClO_4)_2$ (magnesium perchlorate) water trap where residual water vapor was removed, prior to introduction to the gas chromatography (GC) column in a stream of ultra-high purity helium carrier gas. The GC separated the SO_2 based on mass, which was then quantified by the elemental analyzer before flowing into the source of the continuous flow mass spectrometer in a stream of ultra-high purity helium. The SO_2 passed into the ion source (thorium filament) and became ionized to SO_2^-. The ions were then passed through negatively charged accelerating plates that propelled them down the flight tube, where a magnet bent the paths of each mass of sulfur into different Faraday cups, set at m/e of 64 and 66. When the ions hit the collector cups they are recorded as electrical pulses, which were integrated and converted to isotope ratios.

For ^{33}S measurements approximately 2-5 mg of Ag_2S was placed in a Ni-reaction container and combusted under a F_2 atmosphere at 250˚C for 8 hours to produce SF_6. The product SF_6 was purified using gas chromatographic (12 inch Hasep-Q column in a TCD) and cryogenic methods. After purification the sample was introduced to the ThermoFinnigan MAT 253 dual inlet gas-source mass spectrometer, where SF_5^+ was produced and measured at m/e of 127, 128, and 129 (Johnston *et al.,* 2005b).

Analysis of Uncertainty

Analytical and chemical uncertainties are based on the processing of sulfate and sulfide standards (NBS127, IAEA S2, and IAEA S3, all referenced to V-CDT) and are <0.3‰ (1σ) for $\delta^{34}S$ by EA-IRMS and 0.34‰ for $\delta^{34}S$ and 0.016‰ for $\Delta^{33}S$ by SF_6. The EA-IRMS analysis includes correcting the data for drift associated with the number of samples run, and is done so with interspersed standard material, typically NBS 127. The drift is a function of the GC column aging and is easily quantifiable. Figure 6 illustrates a typical EA-IRMS run, uncorrected.

Results

All of the data are reported in Table 1 and plotted in Figure 5. Overall, $\delta^{34}S$ shows broad up-section enrichment. The Minto Inlet Formation shows moderately positive $\delta^{34}S$ values for the evaporites, with a noticeable 5‰ positive shift towards the top of this formation. The range of $\delta^{34}S$ isotopic compositions is from 15.42‰ to 20.46‰ (Figure 5). The minor sulfur isotopic component in this formation shows a large difference in $\Delta^{33}S$ values ranging from -0.034‰ to 0.069‰. The overlying evaporite member (Kilian Formation) exhibits a large $\delta^{34}S$ enrichment that spans 15‰ from 15.46‰ to 30.13‰. The $\Delta^{33}S$ for the Kilian formation exhibit a range of values from -0.003‰ to 0.018‰ with a negative trend (Figure 5).

Discussion

The Neoproterozoic Era is a time of major earth surface changes, with previous C-isotope work suggesting that the Shaler Supergroup may be glacially related (Kaufman and Knoll, 1995). The large negative carbon isotopic excursion in the Kilian Formation, as observed in Figure 5, is strikingly similar to other preglacial sequences including the Otavi group in Namibia (Hoffman *et al.,* 1998), and the Mackenzie Mountains Supergroup in Western Canada (James *et al.,* 2001). Since the Mackenzie Mountains Supergroup was in close proximity to the Shaler Supergroup in the Neoproterozoic (Walter *et al.,* 2000), the Shaler Supergroup is thought to have also recorded the Sturtian glaciation. Also, both supergroups were deposited within the defined age constraints of the Sturtian event. If this large carbon isotopic shift is a preglacial signal, then the sulfur cycle should strongly respond, either through biological limitations (colder temperatures) or basin scale physical properties (a closed basin and pyrite burial). We investigate these through the analyses of bedded evaporites and in the future, the further inclusion of trace sulfate. Carbonate associated sulfate, coupled with lithologic evidence, will be especially important because of the coincidence with the negative carbon isotope excursion observed in the Kilian Formation.

Sulfur isotopic compositions for proxies of seawater sulfate in the Shaler Supergroup are isotopically enriched in $\delta^{34}S$ throughout (Figure 5). This suggests an increase in the amount of sulfide being produced by sulfate reducing bacteria and buried when chemically combining with iron. Coupled with this interpretation is the decrease in the burial of organic carbon, which is consumed in the bacterial metabolisms. The minor sulfur isotope data show a notable transition from one depositional environment to another among the two evaporite rich formations. Large ranges of variability in $\Delta^{33}S$ (0.103‰) further suggests a fundamental change in the operation of the surface sulfur cycle (Figures 8a and 8b, Table 1). Using Figure 7, which is modeled from Johnston *et al.,* (2005a), most (21 of 23) samples, from the Shaler Supergroup plot within the sulfur disproportionation and sulfate reduction field. However, variability in both the reoxidation and pyrite burial pathways suggests a change in the evaporite rich formations.

The Minto Inlet Formation records cyclical variability in the $\delta^{34}S$, which may suggest fluctuations in the availability of sulfur in the system (Figure 5). The mechanisms that cause these fluctuations are pyrite burial and reoxidation of sulfide. Fortunately, minor sulfur isotope measurements allow for the distinction between these mechanisms (Inset in Figure 7). If the sulfur system is physically driven, the variability could be due to changes in oxidative weathering rates or riverine fluxes, which would affect the amount of source sulfate coming into the oceans. This could increase pyrite burial, if the amount of source sulfate decreased, because the sulfur bacteria would have a limited energy source, and as a result more sulfide would be deposited as pyrite. If the system is biologically driven, there would be an increase in reoxidation rates, and both are glacially related. Values of $\Delta^{33}S$ from the Minto Inlet Formation suggest an increase in the amount of sulfide that is being reoxidized in the system (Figure 8a). Increased reoxidation is interpreted as an increase in biological activity, meaning that more sulfide oxidizing bacteria are producing more sulfur intermediates that can be utilized by sulfur

disproportionating bacteria. Conversely, there is a minimal change in the amount of pyrite buried suggesting that the basin did not change. This could be due to high seawater sulfate concentrations, or constant Fe fluxes to the basin which could constrain pyrite formation and deposition. These observations favor a biologically driven environment, where more sulfate is available and bacteria are more active.

The Kilian Formation exhibits a drastic increase in $\delta^{34}S$ of ~15‰ (Figure 5), while preserving relative constant $\Delta^{33}S$ values (~0.044‰) (Figure 8b, Table 1). Traditional $\delta^{34}S$ interpretations would suggest that the isotopic variability is due to an increase in the burial of pyrite in the system. Increases in pyrite burial may suggest the onset of more reducing conditions. Coupled with this large positive isotopic excursion is an equally extreme negative shift in the carbon isotopes at the same stratigraphic level (Figure 5). These two strong lines of isotopic evidence are indicative of a major environmental change, such as a glacial interval. The response of the environment to glacially related effects would include a potential loss of biological life, the progressive decline of oxygen concentrations in the oceans, and the increase of reduced elements like iron and molybdenum in the oceans due to a decrease in sea level because of the formation of continental or polar ice. When the $\Delta^{33}S$ data is interpreted in the context of previous modeling, the trend we observe is an increase in pyrite burial (Figure 8b). These observations lead to environmentally driven changes in the sulfur cycle, which would support the preglacial interpretation.

Even though evidence for sulfur disproportionation reactions was recently found in the middle of the Proterozoic (Johnston *et al.,* 2005a), the significant increase in the fractionation of the sedimentary sulfides in $\delta^{34}S$ is observed at the time the Shaler Supergroup was deposited (Figure 2). Whereas sedimentary sulfides, which record the increase in $\delta^{34}S$, are products of local processes, the sea water sulfate reservoir utilizes the oxidized portion of the sulfur cycle, which is a more direct way of detecting changes in large scale events like glaciations. Perhaps, the drastic changes in the sulfur isotopic record could directly reflect a step-wise change in pO_2 over time.

The activation of a "modern" oxidative sulfur cycle may have been coincident with a second rise in atmospheric oxygen. Based on the Sr isotope record, at the time the Shaler Supergroup was deposited, the deep oceans were potentially anoxic (sulfidic). This oxygenation would have affected the deep oceans as well as the photosynthetic sulfide oxidizers. If the oceans were potentially anoxic (sulfidic) the photosynthetic sulfide oxidizers could have been present in the sea water column which would allow them to be more effective. The nonphotosynthetic sulfide oxidizers, which were confined to the sediments, had a reduced role in the sulfide oxidation process while the photosynthetic sulfide oxidizers were active. If there was a step-wise change in oxygen concentrations in the oceans and the oceans became oxic, then the photosynthetic sulfide oxidizers would have a reduced role, and the nonphotosynthetic sulfide oxidizers would become more abundant and active. Since sulfur disproportionation was active at 1300 Ma. (Johnston *et al.,* 2005a) the large increase in fractionation in the sedimentary sulfide record could be due to this change in activity from photosynthetic sulfide oxidizers to nonphotosynthetic sulfide oxidizers. Also, we could be observing the development of

elemental sulfur disproportionation because elemental sulfur is insoluble, so it would accumulate at the sediment-water interface. As the oceans are progressively changing from anoxic (sulfidic) to oxic, and forcing the advancement of nonphotosynthetic sulfide oxidizers, the sulfur bacteria within the Shaler Supergroup could be dominated by the development of elemental sulfur disproportionating bacteria. Even though this is not the first occurrence of sulfur disproportionators and the oxidative sulfur cycle, their presence may be proportional to the concentrations of oxygen in the atmosphere and oceans. Also, the widespread and pervasive development of sulfur disproportionating bacteria with time, starting with photosynthetic sulfide oxidizers and progressing to nonphotosynthetic sulfide oxidizers, could be a potential reason for the increase in fractionation in the sedimentary sulfide $\delta^{34}S$ record around 800 Ma.

Conclusions

This study set out to find evidence for sulfur disproportionating bacteria at a time period in earth history when there was a large increase in fractionation of sedimentary sulfides. The Shaler Supergroup was deposited around the time a known worldwide glaciation, a glaciation that may be evident in the uppermost formation based on the carbon isotopic analyses. We observed through the use of sulfur isotopes, that the Shaler Supergroup exhibits evidence of a preglacial environment, and that sulfur disproportionating bacteria were present in the Neoproterozoic Era. The presence of sulfur disproportionating bacteria may be proportional to the concentrations of oxygen in the atmosphere and oceans. The widespread and pervasive development of sulfur disproportionating bacteria with time, starting with photosynthetic sulfide oxidizers and progressing to nonphotosynthetic sulfide oxidizers, could be a potential reason for the increase in fractionation in the sedimentary sulfide $\delta^{34}S$ record around 800 Ma. This study is a novel application of minor sulfur isotopes in the formations of the Shaler Supergroup with the Minto Inlet Formation exhibiting a biologically dominant environment based on the data and calculations of $\Delta^{33}S$ and the projection of these data on a previously defined model from Johnston *et al.,* (2005a) (Figure 8a). In the Kilian Formation, the data and calculations suggest environmentally driven changes in the sulfur cycle were dominant based on the same model (Figure 8b). The mechanisms that could drive these environments to be biologically or environmentally dominant could be the effects of oncoming glaciation, a significant change in any of the inputs or outputs within the sulfur cycle (Figure 1) such as a decrease in the amount of weathering or oxidation of the continents and riverine input of source sulfate into the oceans, or changes in the chemistry of the oceans (anoxic (sulfidic) to oxic) in response to the step-wise oxygenation of the atmosphere. Coupled with the modeling, measurements of the sulfur isotopes provide a powerful tool that can resolve changes in the Earth's dynamic biosphere.

Acknowledgments

I want to thank A. J. Kaufman for offering me such an intriguing project, providing the samples for this senior thesis, the use of his laboratory and equipment, his superb

comments and suggestions on my drafts as well as presentations, and help in shaping this extraordinary project.

I want to thank D. Johnston for his tireless work running samples, his extremely helpful comments and suggestions on my papers, presentations, and in the laboratory, and the numerous hours spent teaching me about everything associated with the sulfur cycle.

I want to thank J. Farquhar for the use of his laboratory, chemicals, and equipment.

Figure Captions

Figure 1. A box model of the surface sulfur reservoirs (from Johnston *et al.,* 2005b). The arrows represent fluxes of material between reservoirs, with biologically mediated reactions shown in red arrows, and inorganic reactions in grey. Sulfate ions are delivered to the oceanic sulfate pool via riverine fluxes from the oxidative weathering of the continents. This sulfate could then be reduced by sulfur reducing bacteria, be precipitated out in sulfate minerals (like evaporites), or become bound in the structure of carbonates. Once the sulfate is reduced to hydrogen sulfide, the sulfide could form pyrite (FeS_2), or be reoxidized to a sulfur intermediate (elemental sulfur, thiosulfate, or sulfite). Sulfur disproportionating bacteria can biologically split the sulfur intermediates into sulfate or hydrogen sulfide.

Figure 2. A plot of $\delta^{34}S$ versus time for sedimentary sulfides (modified from Canfield 2001). The upper black lines represent the modeled seawater sulfate curve with a 5‰ uncertainty, whereas the lower line is seawater sulfate offset by 55‰. The dashed red box represents the approximate position of the Shaler Supergroup. The solid red contours reflect estimations of the total $\delta^{34}S$ fractionation expressed, with A = ~46‰ and B = ~71‰.

Figure 3a. A political map of Canada displaying all of the territories, with the Shaler Supergroup located in the Northwest Territories section of Victoria Island (marked by *).
Figure 3b. A picture of the Shaler Supergroup outcrop provided by Alan J. Kaufman.

Figure 4. Prior isotopic measurements on the Shaler Supergroup plotted against depth, on the Shaler Supergroup. The simplified lithology was based on Young (1981), Rainbird (1991) (unpublished PhD dissertation), and Rainbird (1992). The carbonate sections are blue rectangles, the siliciclastic sections are green rectangles, the evaporite sections are yellow rectangles, and the shale sections are black rectangles. The size of the rectangles makes the column easier to understand. The $\delta^{13}C_{TOC}$ data were unpublished and provided by Alan J. Kaufman (personal communication), and the symbols are yellow triangles pointing up. The $\delta^{18}O_{carb}$ data are unpublished and provided by Alan J. Kaufman (personal communication), and the symbols are blue triangles. The triangles that are pointing down represent carbonate samples, and the triangles that are pointing up represent dolomite samples. The $\delta^{13}C_{carb}$ data are from Kaufman and Knoll, (1995), and the symbols are black and white triangles. The $\delta^{13}C_{carb}$, $\delta^{13}C_{TOC}$, $\delta^{18}O_{carb}$ data are relative to the (V-PDB) Vienna Pee Dee Belemnite scale. The black triangles represent dolomite samples and the white triangles represent carbonate samples. The $^{87}Sr/^{86}Sr$ data are from Asmerom *et al.,* (1991), (red circles).

Figure 5. **S**hown are the sulfur isotopic compositions on the Shaler Supergroup with the carbon isotopic data from Figure 4 included for reference. The $\delta^{13}C_{TOC}$ data are from Alan J. Kaufman (personal communication), and the $\delta^{13}C_{carb}$ data are from Kaufman and Knoll, (1995). The red dots represent data from evaporite samples. The star symbols represent the $\Delta^{33}S$ isotopic data that was obtained from evaporite samples (isotopic compositions are relative to the V-CDT (Vienna Canyon Diablo Troilite) scale). The

simplified stratigraphic column was based on Young (1981), Rainbird (1991) (unpublished PhD dissertation), and Rainbird (1992).

Figure 6. An illustration showing the $\delta^{34}S$ drift versus the sample number run. From this regression, a correction factor relating sample to drift, is calculated. Measurements via EA-IRMS drift are due to the GC column.

Figure 7. $\Delta^{33}S$ versus $\delta^{34}S$ compositions for seawater sulfate produced from an open-system steady-state five box surface sulfur cycle model (from Johnston *et al.* 2005a). The isotopic signature produced by sulfate reducing bacteria is in the red field. The characteristic sulfur disproportionating bacteria and sulfate reducing bacteria field is shaded blue. The arrows in the bottom right represent the direction that $\Delta^{33}S$ and $\delta^{34}S$ compositions evolve with increasing pyrite burial (f_{py}) and sulfide re-oxidation ($f_{r\text{-}o}$). These fields are used to evaluate the presence of these bacteria in the sulfur cycle during deposition (Johnston *et al.*, 2005b). All isotopic compositions are relative to V-CDT (Vienna Canyon Diablo Troilite) scale.

Figure 8a. This figure represents the evaporite data measured from the Minto Inlet Formation within the Shaler Supergroup. Sulfate fields are from Figure 7. The size of the symbols encompasses any error in $\delta^{34}S$.

Figure 8b. This figure represents the evaporite data measured from the Kilian Formation within the Shaler Supergroup. Sulfate fields are from Figure 7. The size of the symbols encompasses any error in $\delta^{34}S$.

Table 1. Sulfur isotope measurements of evaporites and carbonate associated sulfate (listed as C under lithology) from sedimentary successions within the Shaler Supergroup. The $\delta^{34}S$ EA-IRMS values were measured with an uncertainty of <0.6‰ (2σ). All other measurements ($\delta^{33}S$ and $\delta^{34}S$) were made on a DI-IRMS with uncertainties of ± 0.34‰ and ± 0.016 (2σ) for $\delta^{34}S$ and $\Delta^{33}S$ respectively. The samples marked with an x need to be reanalyzed due to complications with the EA-IRMS.

Figures and Table

Figure 1

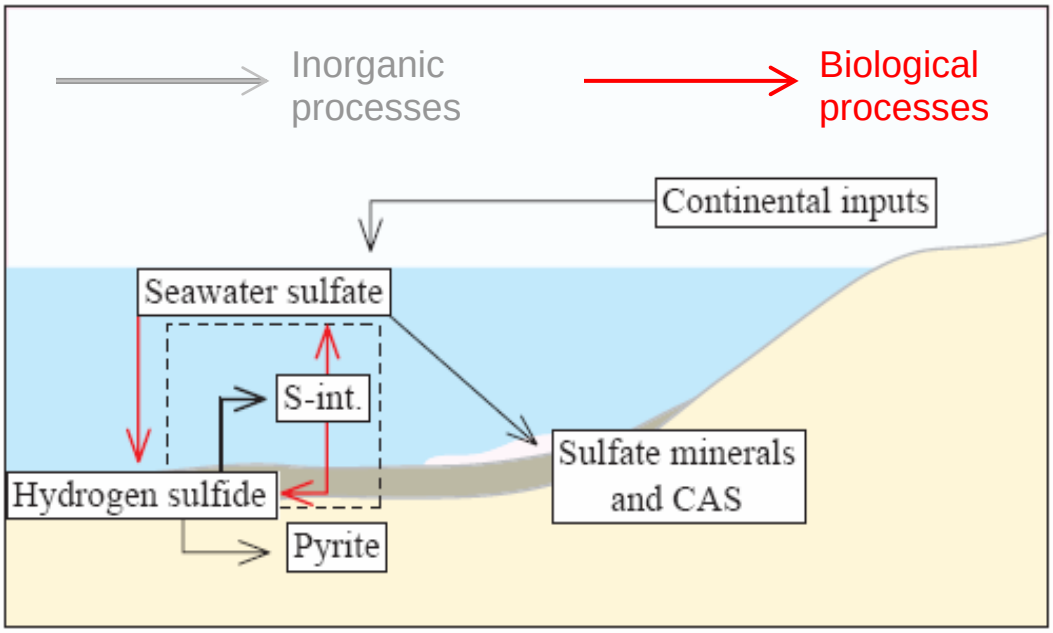

Figure 2

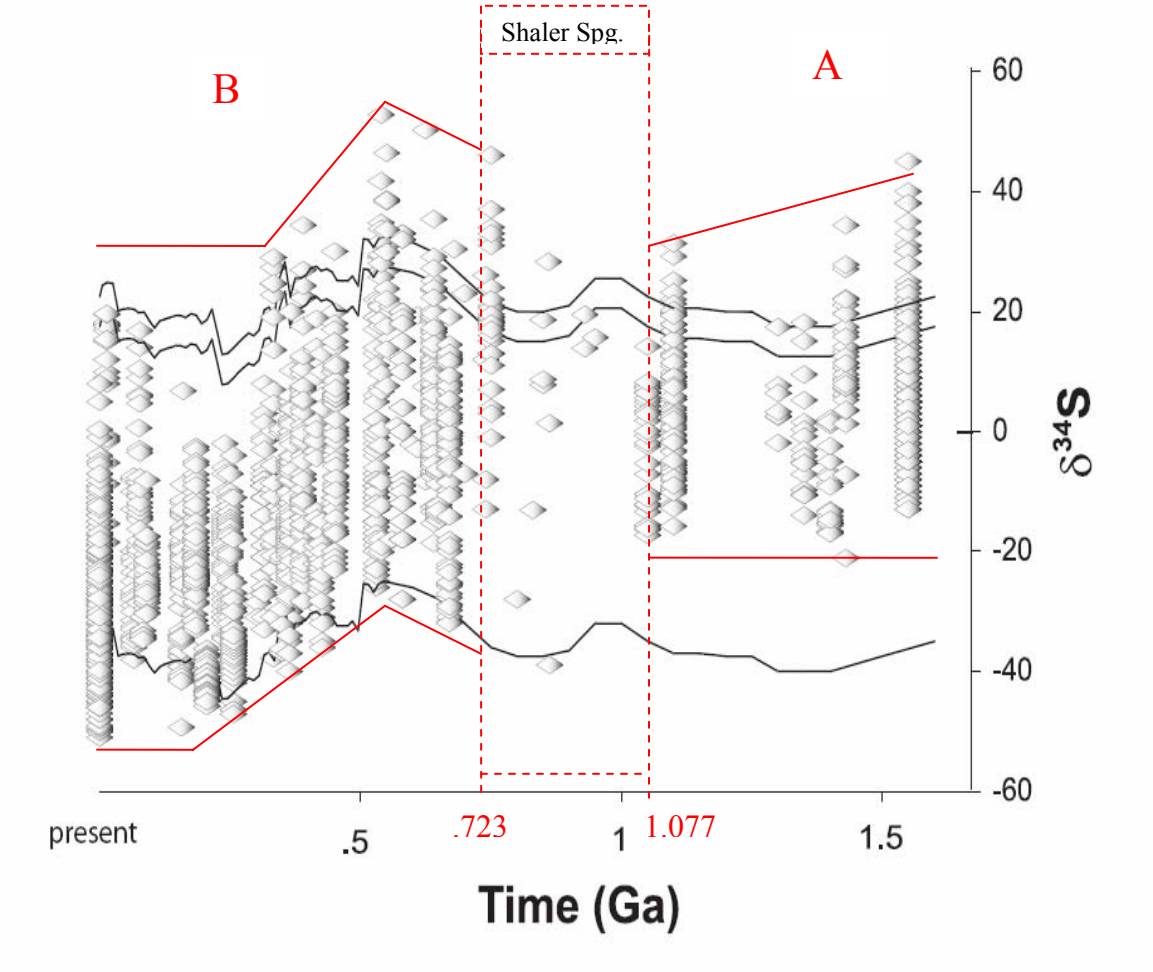
Shaler Spg.
B
A
60
40
20
0
-20
-40
-60
$\delta^{34}S$
present
.5
.723
1
1.077
1.5
Time (Ga)

Figure 3

a. b.


North Pole
Norwegian Sea
Norway
Polar Ice
Greenland Sea
UK
Russia
Arctic Ocean
Ellesmere Island
Alert
Kalaallit Nunaat (Grønland) (Denmark)
Iceland
North Magnetic Pole
Arctic Circle
Alaska (USA)
Beaufort Sea
Banks I.
Resolute
Baffin Bay
Inuvik
Victoria Island
Gjoa Haven
Baffin Island
Davis Strait
Dawson
Great Bear Lake
Yukon Territory
Whitehorse
Mackenzie River
Northwest Territories
Nunavut
Iqaluit
Labrador Sea
Baker Lake
Yellowknife
Great Slave Lake
Fort Nelson
CANADA
Atlantic Ocean
Ungava B. Bay
Nain
Newfoundland
British Columbia
Prince George
Fort McMurray
Alberta
Edmonton
Saskatchewan
Churchill
Manitoba
Hudson Bay
Kuujjuaq
Churchill Falls
St John's
Pacific Ocean
Fraser River
Vancouver
Victoria
Kamloops
Calgary
Saskatoon
Regina
Winnipeg
Sandy Lake
James Bay
La Grande Rivière
Sept-Îles
Saint-Pierre et Miquelon (France)
Quebec
Prince Edward Island
Charlottetown
New Brunswick
Nova Scotia
Halifax
Fredericton
Québec
Thunder Bay
Ontario
Montréal
United States of America
Ottawa
Toronto
Lake Superior
Lake Michigan
Lake Huron
Lake Ontario
Lake Erie
LEGEND
National capital
Provincial or Territorial capital
Other populated places
Scale
300 0 300 600 900 km
© 2000. Her Majesty the Queen in Right of Canada, Natural Resources Canada.

Figure 4

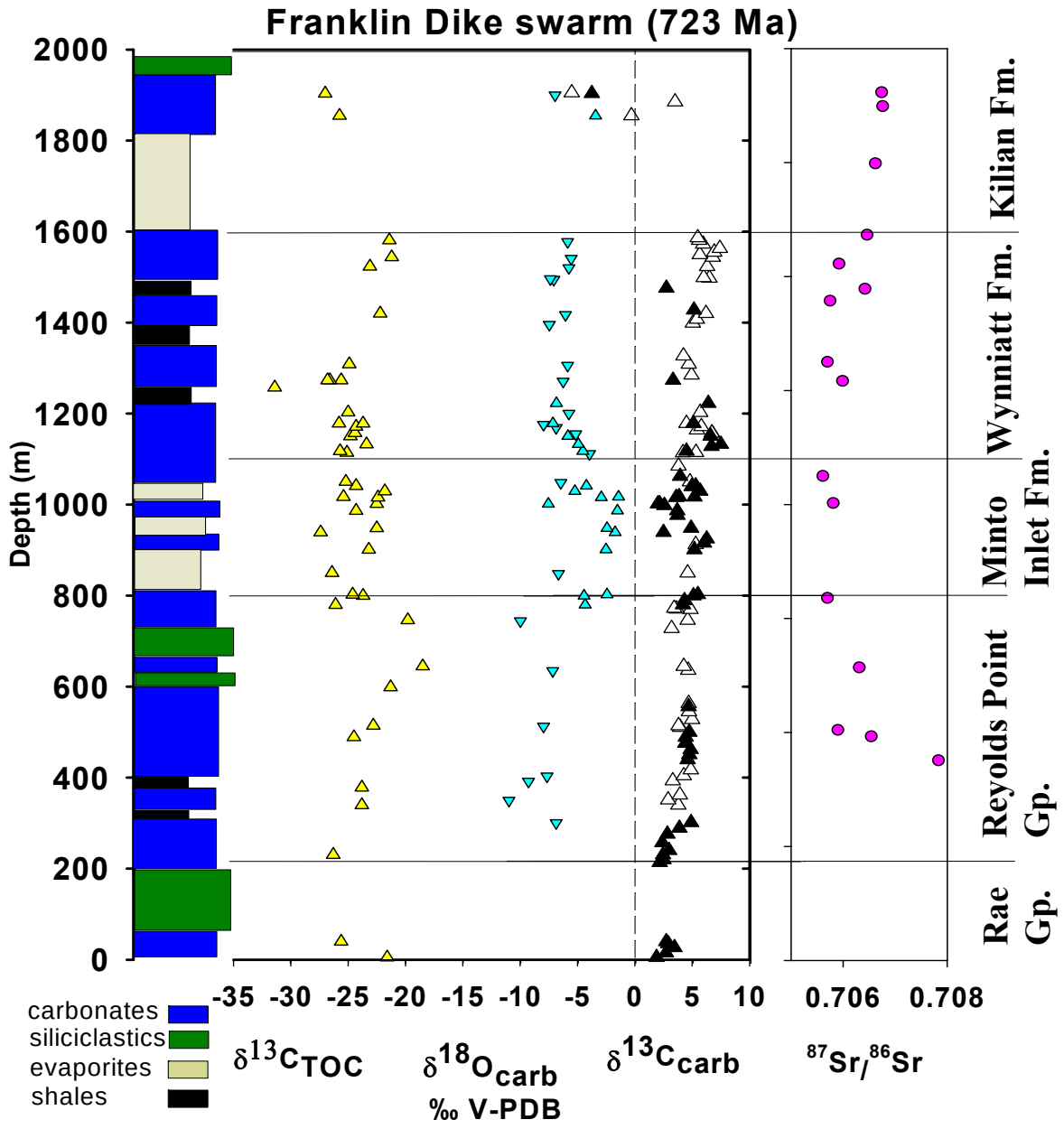
Franklin Dike swarm (723 Ma)
Depth (m)
2000
1800
1600
1400
1200
1000
800
600
400
200
0
Kilian Fm.
Wynniatt Fm.
Minto Inlet Fm.
Reyolds Point Gp.
Rae Gp.
carbonates
siliciclastics
evaporites
shales
-35 -30 -25 -20 -15 -10 -5 0 5 10
0.706 0.708
δ13CTOC
δ18Ocarb
δ13Ccarb
87Sr/86Sr
‰ V-PDB

Figure 5

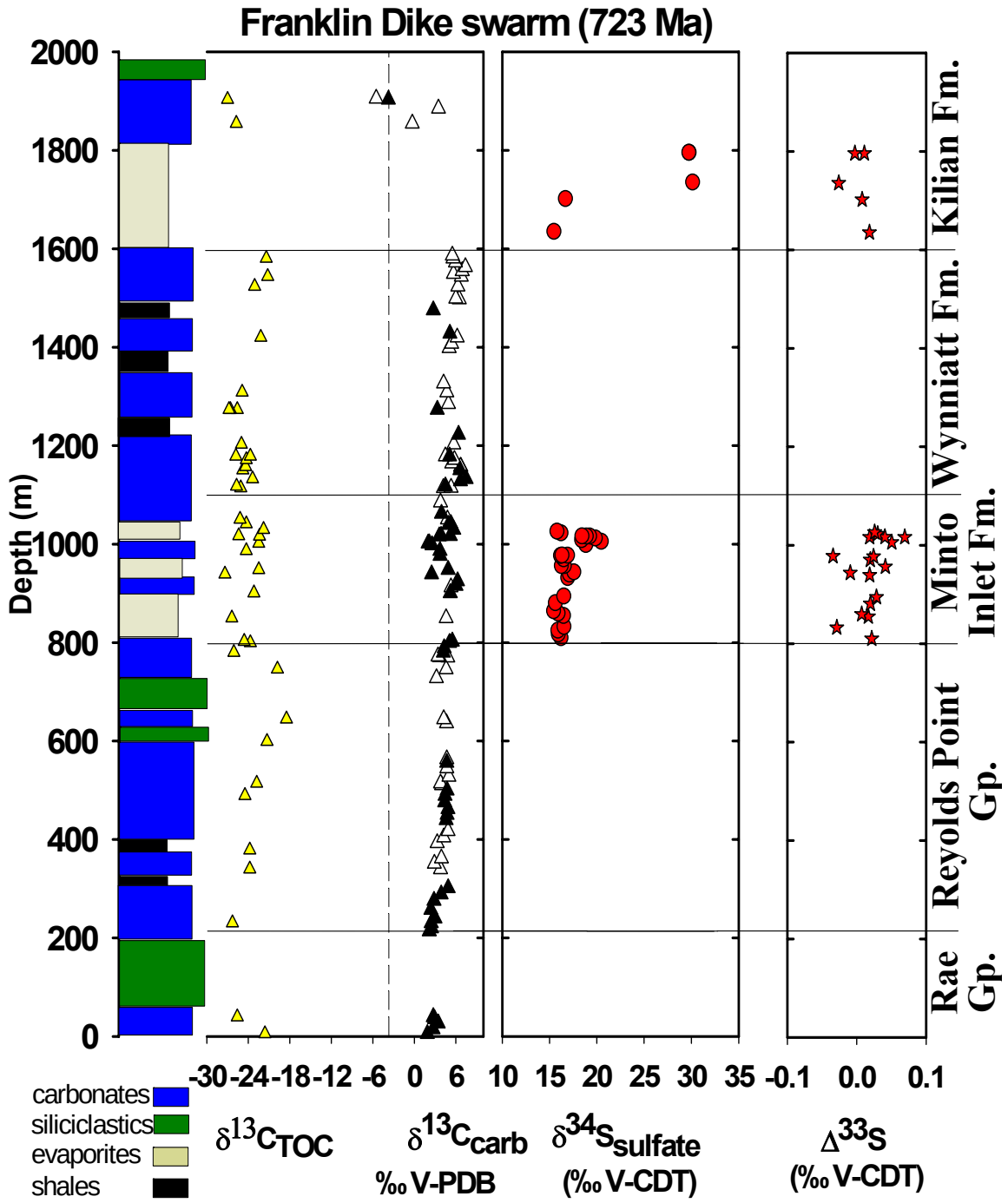
Franklin Dike swarm (723 Ma)
Depth (m)
2000
1800
1600
1400
1200
1000
800
600
400
200
0
Kilian Fm.
Wynniatt Fm.
Minto Inlet Fm.
Reyolds Point Gp.
Rae Gp.
carbonates
siliciclastics
evaporites
shales
-30 -24 -18 -12 -6 0 6
δ13CTOC
10 15 20 25 30 35
δ13Ccarb
‰ V-PDB
δ34Ssulfate
(‰ V-CDT)
-0.1 0.0 0.1
Δ33S
(‰ V-CDT)

Figure 6

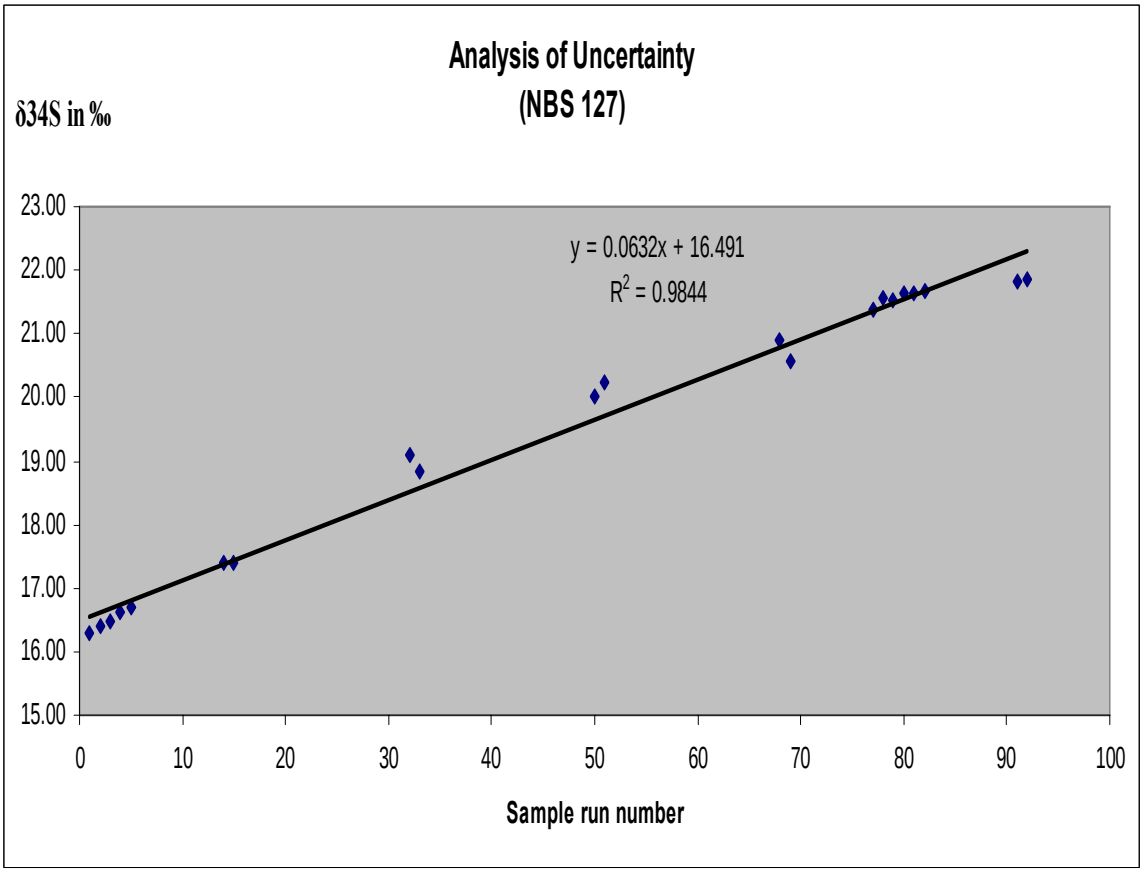
Analysis of Uncertainty
(NBS 127)
δ34S in ‰
y = 0.0632x + 16.491
R2 = 0.9844
23.00
22.00
21.00
20.00
19.00
18.00
17.00
16.00
15.00
0
10
20
30
40
50
60
70
80
90
100
Sample run number

Figure 7

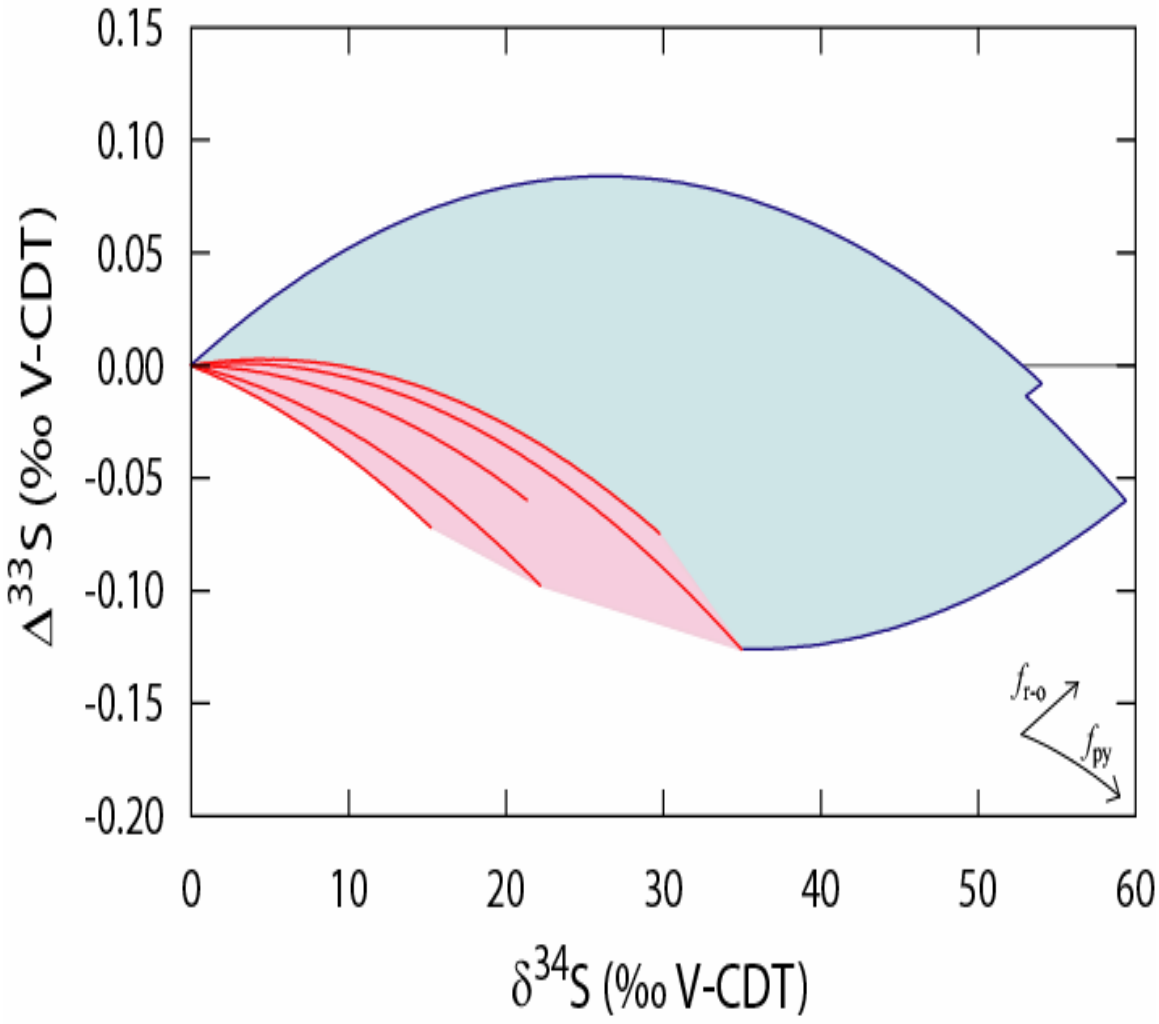
0.15
0.10
0.05
0.00
-0.05
-0.10
-0.15
-0.20
$\Delta^{33}S$ (‰ V-CDT)
0
10
20
30
40
50
60
$\delta^{34}S$ (‰ V-CDT)
$f_{r\text{-}o}$
f_{py}

Figure 8a

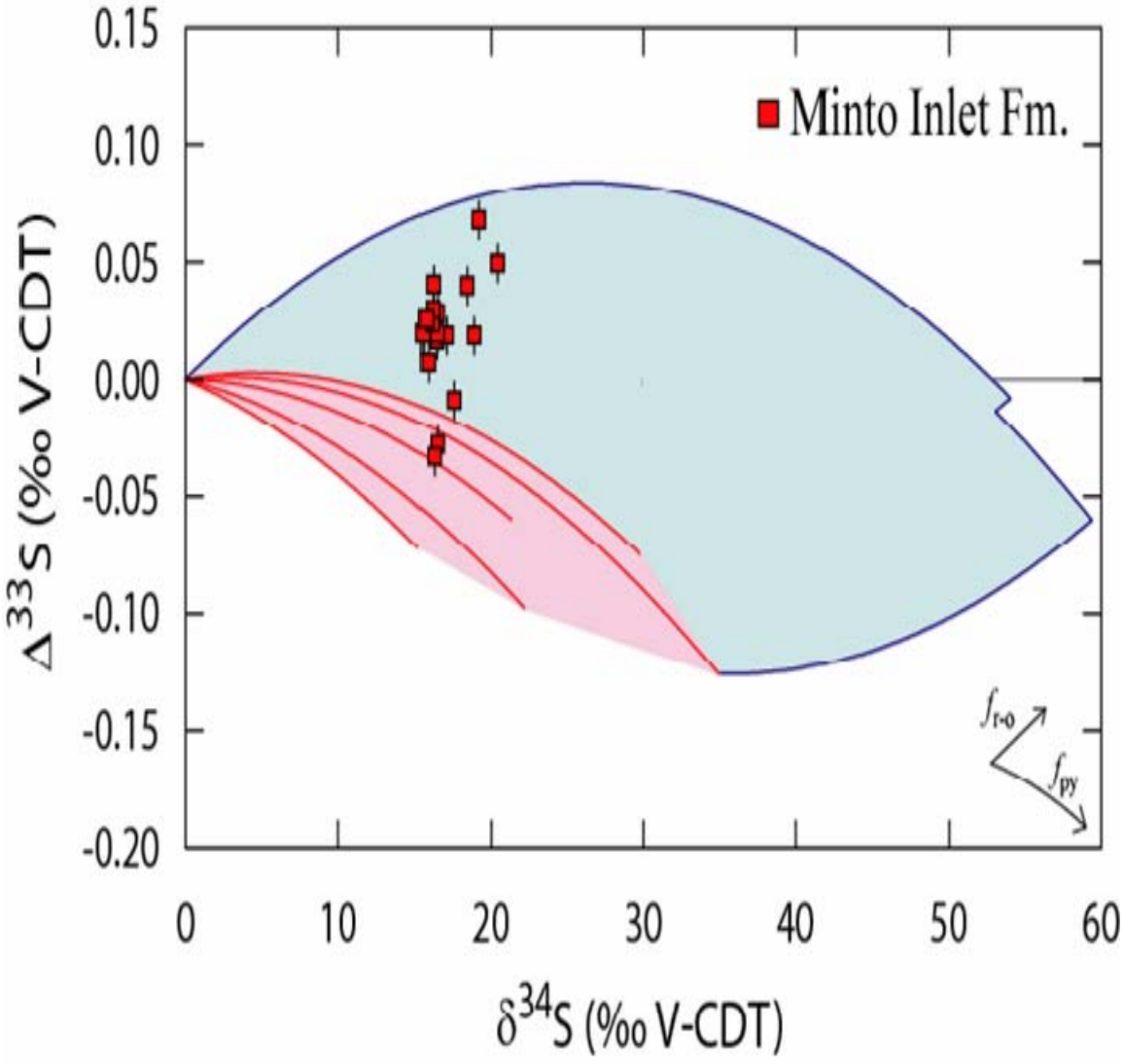
Minto Inlet Fm.
0.15
0.10
0.05
0.00
-0.05
-0.10
-0.15
-0.20
0
10
20
30
40
50
60
Δ33S (‰ V-CDT)
δ34S (‰ V-CDT)
fr-o
fpy

Figure 8b

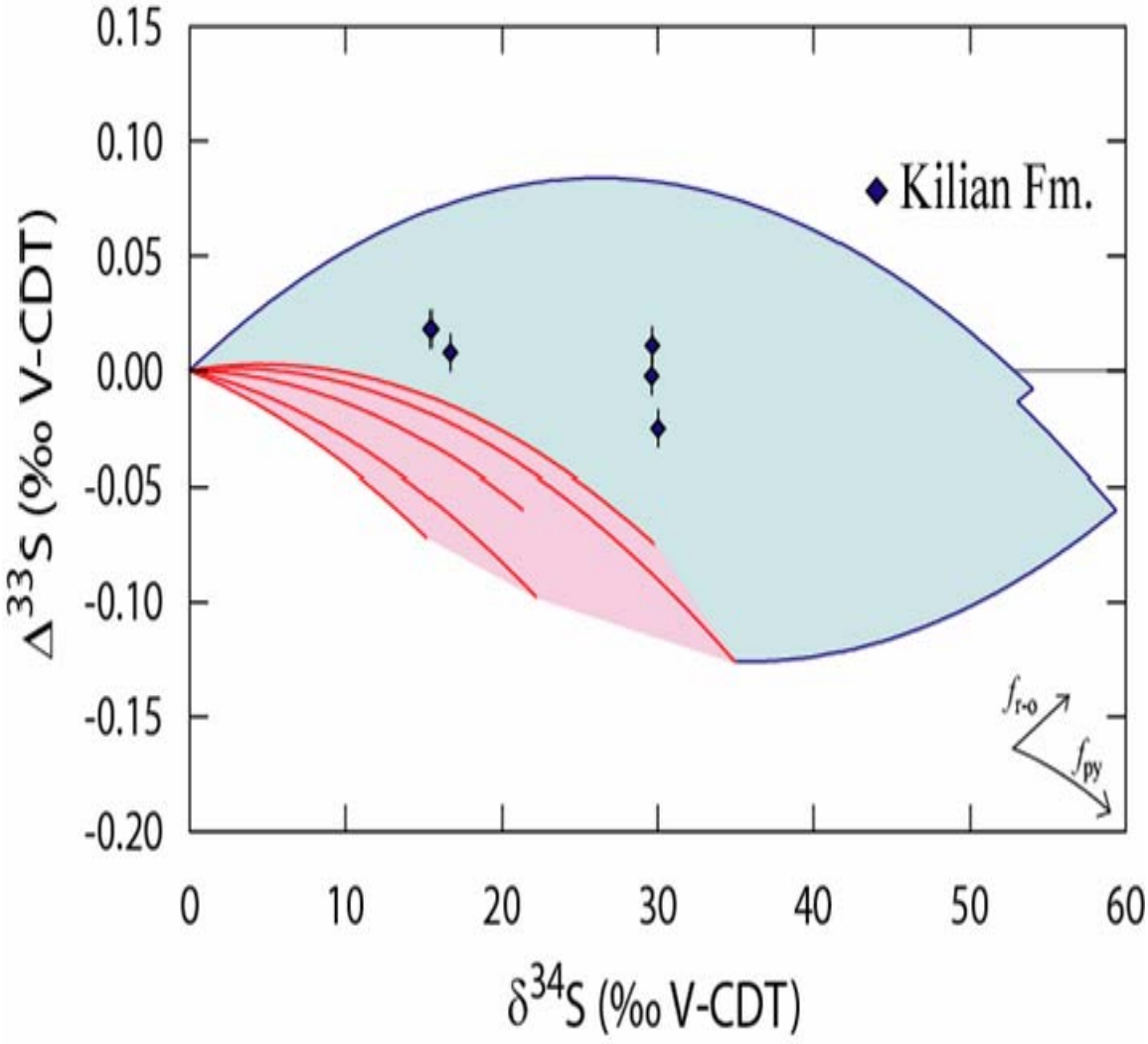
0.15
0.10
0.05
0.00
-0.05
-0.10
-0.15
-0.20
Δ33S (‰ V-CDT)
0
10
20
30
40
50
60
δ34S (‰ V-CDT)
Kilian Fm.
fr-o
fpy

Table 1

Formation	Depth (m)	Sample	$\delta^{34}S$ (‰)	$\Delta^{33}S$ (‰)
Kilian Fm.	1795.9	KL 150P	29.76	0.011
Kilian Fm.	1795.9	KL 150S	29.73	-0.003
Kilian Fm.	1735.58	KL 148	30.13	-0.026
Kilian Fm.	1702.16	KL 136	16.68	0.008
Kilian Fm.	1635.32	KL 134	15.46	0.018
Minto Inlet Fm.	1026.23	GB 52	15.78	0.026
Minto Inlet Fm.	1022.77	GB 51	16.21	0.030
Minto Inlet Fm.	1016.675	KL 99	18.43	0.041
Minto Inlet Fm.	1016.45	KL 98	18.89	0.019
Minto Inlet Fm.	1016.225	KL 97	19.23	0.069
Minto Inlet Fm.	1012.55	GB 48	19.84	
Minto Inlet Fm.	1009.1	GB 47	18.39	
Minto Inlet Fm.	1005.65	GB 45	20.46	0.051
Minto Inlet Fm.	999.15	GB 42	18.84	
Minto Inlet Fm.	977.725	GB 54	16.31	-0.034
Minto Inlet Fm.	977.35	GB 39	16.90	
Minto Inlet Fm.	976.975	GB 38	16.16	0.024
Minto Inlet Fm.	970.35	GB 36	16.49	0.020
Minto Inlet Fm.	956.15	GB 33L	16.56	
Minto Inlet Fm.	956.15	GB 33D	16.24	0.041
Minto Inlet Fm.	943.65	GB 30	17.57	-0.009
Minto Inlet Fm.	939.1	GB 27	17.10	0.019
Minto Inlet Fm.	931.95	GB 26	16.93	
Minto Inlet Fm.	894.35	GB 18	16.50	0.029
Minto Inlet Fm.	881.05	GB 16	15.61	0.020
Minto Inlet Fm.	864.64	GB 13	15.42	
Minto Inlet Fm.	859.76	GB 12	15.91	0.007
Minto Inlet Fm.	854.88	GB 11	16.47	0.017
Minto Inlet Fm.	832.66	GB 8	16.52	-0.029
Minto Inlet Fm.	825.12	GB 7	15.89	
Minto Inlet Fm.	817.58	GB 5	15.92	
Minto Inlet Fm.	810.04	GB 4	16.21	0.022

Bibliography

Asmerom, Y., Jacobsen, S. B., Knoll, A. H., Butterfield, N. J., Swett, K., 1991. Strontium isotopic variations of Neoproterozoic seawater: Implications for crustal evolution. Geochimica et Cosmochimica Acta, v. 55, p. 2883–2894.

Canfield, D. E., 1998. A new model for Proterozoic ocean chemistry. Nature, v. 396, p. 450–453.

Canfield, D. E., 2001. Biogeochemistry of sulfur isotopes, in J. W. Valley, D. R. Coles eds., Stable Isotope Geochemistry. Reviews in Mineralogy and Geochemistry, v. 43, p. 607-636.

Canfield, D. E. and Raiswell, R., 1999. The evolution of the sulfur cycle. American Journal of Science, v. 299, p. 697–723.

Canfield, D. E. and Teske, A., 1996. Late Proterozoic rise in atmospheric oxygen concentration inferred from phylogenetic and sulphur-isotope studies. Nature, v. 382, p. 127–132.

Canfield, D. E., 1997. Sulfur isotope fractionation during bacterial sulfate reduction in organic-rich sediments. Geochimica et Cosmochimica Acta, v. 61, no. 24, p. 5351-5361.

Chambers, L. A., Trudinger, P. A., Smith, J. W., Burns, M. S., 1976. Possible boundary-condition in bacterial sulfur isotope fractionation. Geochimica et Cosmochimica Acta, v. 40, p. 1191–1194.

Dalziel, I.W.D., 1997. Overview: Neoproterozoic-Paleozoic geography and tectonics: Review, hypothesis, environmental speculations. Geological Society of America Bulletin, v. 109, p. 16–42.

Dehler, C. M., Elrick, M., Bloch, J.D., Crossey, L.J., Karlstrom, K.E., Des Marais, D. J., 2005. High-resolution $\delta^{13}C$ stratigraphy of the Chuar Group (ca. 770 –742 Ma), Grand Canyon: Implications for mid-Neoproterozoic climate change. GSA Bulletin, v. 117, no. 1/2, p. 32–45.

Detmers, J., Bruchert, V., Habicht, K. S., Kuever, J., 2001. Diversity of Sulfur Isotope Fractionations by Sulfate-Reducing Prokaryotes. Applied and Environmental Microbiology, v. 67, no. 2, p. 888–894.

Ding, T., Valkiers, S., Kipphardt, H., De Bièvre, P., Taylor, P. D. P., Gonfiantini, R., Krouse, R., 2001. Calibrated sulfur isotope abundance ratios of three IAEA sulfur isotope reference materials and V-CDT with a reassessment of the atomic weight of sulfur. Geochimica et Cosmochimica Acta, v. 65, no. 15, p. 2433-2437.

Farquhar, J., Johnston, D. T., Wing, B. A., Habicht, K. S., Canfield, D. E., Airieau, S.,

Thiemens, M. H., 2003. Multiple sulphur isotopic interpretations of biosynthetic pathways: implications for biological signatures in the sulphur isotope record. Geobiology, v. 1, p. 27-36.

Gorjan, P., Veevers, J. J., Walter, M.R., 2000. Neoproterozoic sulfur-isotope variation in Australia and global implications. Precambrian Research, v. 100, p. 151-179.

Habicht, K. S., Canfield, D. E., 1997. Sulfur isotope fractionation during bacterial sulfate reduction in organic-rich sediments. Geochimica et Cosmochimica Acta, v. 61, no. 24, p. 5351-5361.

Habicht, K. S., Canfield, D. E., Rethmeier, J., 1998. Sulfur isotope fractionation during bacterial reduction and disproportionation of thiosulfate and sulfite. Geochimica et Cosmochimica Acta, v. 62, no. 15, p. 2585–2595.

Habicht, K. S., Canfield, D. E., 2002. Isotope fractionation by sulfate-reducing natural populations and the isotopic composition of sulfide in marine sediments. Geology, v. 29, p. 555-558.

Habicht, K. S., Gade, M., Thamdrup, B., Berg, P., Canfield, D. E., 2002. Calibration of sulfate levels in the Archean ocean. Science, v. 298, no. 5602, p. 2372-2374.

Harrison, A. G., Thode, H. G., 1958. Mechanism of the bacterial reduction of sulphate from isotope fractionation studies. Transactions of the Faraday Society, v. 54, p. 84-92.

Hoefs, J., 2004. Stable Isotope Geochemistry. Pub. Springer. 5th ed. p. 244.

Hoffman, P. F., Kaufman, A. J., Halverson, G. P. and Schrag, D. P., 1998. A Neoproterozoic snowball Earth. Science, v. 281, p. 1342–1346.

Hoffman, P. F., 1991. Did the Breakout of Laurentia Turn Gondwanaland Inside Out. Science, v. 252, no. 5011, p. 1409-1412.

Holser, W. T., 1977. Catastrophic chemical events in the history of the ocean. Nature, v. 267, p. 403-408.

Hulston, J. R., Thode, H. G., 1965. Cosmic ray produced ^{36}S and ^{33}S in metallic phase of Iron Meteorites. Journal of Geophysical Research, v. 70, p. 4435-4442.

Hurtgen, M. T., Arthur, M. A., Halverson, G. P., 2005. Neoproterozoic sulfur isotopes, the evolution of microbial sulfur species, and the burial efficiency of sulfide as sedimentary pyrite. Geology, v. 33, no. 1, p. 41-44.

Hurtgen, M. T., Arthur, M. A., Prave, A. R., 2004. The sulfur isotopic composition of

carbonate-associated sulfate in Mesoproterozoic to Neoproterozoic carbonates from Death Valley, California. In: Amend, J. P., Edwards, K. J., Lyons, T. W., eds., Sulfur Biogeochemistry-Past and Present: Geological Society of America Special Paper 379, p. 177-194.

Hurtgen, M. T., Arthur, M. A., Suits, N. S., Kaufman, A. J., 2002. The sulfur isotopic composition of Neoproterozoic seawater sulfate: implications for a snowball Earth? Earth and Planetary Science Letters 203, p. 413-429.

Hulston, J., R., Thode, H. G., 1965. Variations in the S (super 33), S (super 34), and S (super 36) contents of meteorites and their relation to chemical and nuclear effects. Journal of Geophysical Research, v. 70, no. 14, p. 3475-3484.

Johnston, D. T., Farquhar, J., Wing, B. A., Kaufman, A. J., Canfield, D. E., Habicht, K. S., 2005a. Multiple sulfur isotope fractionations in biological systems, American Journal of Science, v. 305, p. 645-660.

Johnston, D. T., Wing, B. A., Farquhar, J., Kaufman, A. J., Strauss, H., Lyons, T. W., Kah, L. C., Canfield, D. E., 2005b. Active microbial sulfur disproportionation in the Proterozoic, Science, v. 310, p. 1477-1479.

Kaplan, I. R., Rittenburg, S. C., 1964. Microbiological fractionation of sulphur isotopes. Journal of General Microbiology, v. 34, p. 195-212.

Kaufman, A. J., Knoll, A. H., 1995. Neoproterozoic variations in the C-isotope composition of seawater: stratigraphic and biogeochemical implications. Precambrian Research, v. 73, p. 27-49.

Kemp, A. L. W., Thode, H. G., 1968. Mechanism of bacterial reduction of sulphate and of sulphite from isotope fractionation studies. Geochimica et Cosmochimica Acta, v. 32, p. 71-91.

Kirschvink, J. L., 1992. Late Proterozoic low-latitude global glaciation: the snowball earth. In: Schopf, J. W., Klein, C., eds., The Proterozoic Biosphere. pp. 51–52. Cambridge University Press, Cambridge.

Karlstrom, K. E., Bowring, S.A., Dehler, C. M., Knoll, A. H., Porter, S. M., Des Marais, D. J., Weil, A. B., Sharp, Z. D., Geissman, J. W., Elrick, M. B., Timmons, J. M., Crossey, L. J., Davidek, K. L., 2000. Chuar Group of the Grand Canyon: Record of breakup of Rodinia, associated change in the global carbon cycle, and ecosystem expansion by 740 Ma. Geology, v. 28, no. 7, p 619-622.

Morin, J., Rainbird, R. H., 1993. Sedimentology and sequence stratigraphy of the Neoproterozoic Reynolds Point Formation, Minto Inlier, Victoria Island, Northwest Territories. Current Research, Part C, Geological Survey of Canada, Paper 93-1C, p. 7-18.

Neretin, L. N., Volkov, I. I., Bottcher, M. E., Grinenko, V. A., 2001. A sulfur budget for the Black Sea anoxic zone. Deep Sea Research I, v. 48, p. 2569-2593.

Ohmoto, H., Kakegawa, T., Lowe, D. R., 1993. 3.4-Billion Year–Old Biogenic pyrites from Barberton, South Africa: Sulfur Isotope Evidence. Science, v. 262, no. 5133, p 555-557.

Pollard, D., Kasting, J. F., 2005. Snowball Earth: A thin-ice solution with flowing sea glaciers. Journal of Geophysical Research, v. 110, p. 1-16.

Rainbird, R. H., Jefferson, C. W., Young, G. M., 1996. The early Neoproterozoic sedimentary Succession B of northwestern Laurentia: Correlations and paleogeographic significance. GSA Bulletin, v. 108, no. 4, p. 454-470.

Rainbird, R. H., Jefferson, C. W., Hildebrand R. S., Worth, J. K., 1994. The Shaler Supergroup and revision of Neoproterozoic stratigraphy in Amundsen Basin, Northwest Territories. Current Research, 1994-C, Geological Survey of Canada, p. 61-70.

Rainbird, R. H., Darch, W., Jefferson, C. W., Lustwerk, R., Rees, M., Telmer, K., Jones, T.A., 1992. Preliminary stratigraphy and sedimentology of the Glenelg Formation, lower Shaler Group and correlatives in the Admundsen Basin, Northwest Territories: relevance to sediment-hosted copper. Current Research, Part C, Geological Survey of Canada, Paper 92-1C, p. 111-119.

Rainbird, R. H., 1991. Stratigraphy, Sedimentology, and Tectonic Setting of the Upper Shaler Supergroup, Northwest Territories, PhD. Thesis, University of Western Ontario. (unpublished)

Schauble, E. A., 2004. Applying stable isotope fractionation theory to new systems. In: Johnson, C. M., Beard, B. L., Albarede, F., eds., Geochemistry of Non-Traditional Stable Isotopes: Reviews in Mineralogy and Geochemistry, v. 55, p. 65-111.

Shen, Y. A., Buick, R., Canfield, D. E., 2001. Isotopic evidence for microbial sulphate reduction in the early Archean era. Nature, v. 410, p. 77-81.

Strauss, H., 1997. The isotopic composition of sedimentary sulfur through time. Paleogeography, Paleoclimatology, Paleoecology, v. 132, p. 97-118.

Strauss, H., Banerjee, D. M., Kumar, V., 2001. The sulfur isotopic composition of Neoproterozoic to early Cambrian seawater — evidence from the cyclic Hanseran evaporites, NW India. Chemical Geology, v. 175, p. 17-28.

Thode, H. G., Monster, J., Dunford, H. B., 1961. Sulphur isotope geochemistry. Geochimica et. Cosmochimica Acta, v. 25, p. 159-174.

Walter, M. R., Veevers, J. J., Calver, C. R., Gorjan, P., Hill, A.C., 2000. Dating the 840–544 Ma Neoproterozoic interval by isotopes of strontium, carbon, and sulfur in seawater, and some interpretative models. Precambrian Research, v. 100, p. 371–433.

Young, G. M., 1981. The Amundsen Embayment, Northwest Territories; relevance to the upper Proterozoic evolution of North America. In: Campbell, F. H. A., ed., Proterozoic Basins of Canada: Geological Survey of Canada, Paper 81-10, p. 203-211.